https://doi.org/10.5194/wes-2023-177
Preprint. Discussion started: 7 March 2024

eawe european academy of wind energy
Open Access WIND ENERGY SCIENCE DISCUSSIONS

Improving Wind and Power Predictions via Four-Dimensional Data Assimilation in the WRF Model: Case Study of Storms in February 2022 at Belgian Offshore Wind Farms

Tsvetelina Ivanova[1,2], Sara Porchetta[1,3], Sophia Buckingham[1], Jeroen van Beeck[1], and Wim Munters[1]

[1]von Karman Institute for Fluid Dynamics, Environmental and Applied Fluid Dynamics Department, 1640 Sint-Genesius-Rode, Belgium
[2]Vrije Universiteit Brussel, Department of Mechanical Engineering, Belgium
[3]Massachusetts Institute of Technology, Civil and Environmental Engineering, 77 Massachusetts Avenue, 1-290, Cambridge, MA 02139, United States of America

Correspondence: Tsvetelina Ivanova (tsvetelina.ivanova@vki.ac.be)

Abstract. Accurate wind and power predictions from numerical models are crucial for wind farm operation and management. This study explores how these predictions can be improved by assimilating local offshore data into a numerical weather prediction model, while simultaneously taking into account the presence of neighboring wind farms. The focus is on the Belgian-Dutch wind farm cluster located in the Southern Bight of the North Sea. Our results show that, for the current case study with extreme weather conditions, the assimilation of upstream data reduces mean absolute errors of wind speed, wind direction, and power predictions, up to 2.7 times in comparison to simulations without any assimilation. This approach can be useful for forecasting purposes in short- to mid-term horizons, as well as for a long-term refined reanalysis of various weather conditions and events.

1 Introduction

In recent years, wind energy has emerged as a crucial and rapidly growing renewable energy source. Accurate predictions of wind speed, wind direction, and power production have become essential for efficient planning, design and operation of wind farms. The use of numerical weather prediction (NWP) models, such as the open-source Weather Research and Forecasting Model (WRF, Skamarock et al. (2019)), developed at the National Center for Atmospheric Research (NCAR), plays a vital role in obtaining these accurate predictions. In the context of wind farm market operations, forecasts of different lead times have different applications (Soman et al., 2010). Short-term forecasts of up to 6 hours ahead serve for regulation, dispatching, and congestion management, whereas mid-term forecasts of days-ahead serve for reserve requirement and market trading. Long-term forecasts of weeks, seasons or more, are useful for resource planning, operation management, optimal maintenance scheduling, and long-term energy trading. In the present study, short-term and mid-term forecasts are of interest. Furthermore, wind is generated due to a number of physical weather processes, which can be simulated accurately only by NWP models (Cheng et al., 2013). This renders the NWP approach more favorable for our goals than statistical models, although these can have strengths especially in post-processing techniques. For offshore wind farms, NWP models do not necessarily have initial

https://doi.org/10.5194/wes-2023-177
Preprint. Discussion started: 7 March 2024

eawe european academy of wind energy
Open Access WIND ENERGY SCIENCE DISCUSSIONS

conditions that are accurate enough due to the sparsity of offshore observations. This lack of data leads to broader issues, where NWP models can display large bias errors due to the overall lack of long-term offshore measurement data (Archer et al., 2014).

Extreme events can have a profound impact on wind farm operations, since they can often lead to implications for power generation and grid stability. The impact at near-ground levels can be damaging for human activity, as well as cause grid instabilities and potential wind turbine cut-outs. Consequently, numerous studies are dedicated to studying and understanding extreme events, such as Larsén et al. (2019), Pryor and Barthelmie (2021), Sethunadh et al. (2023), Vemuri et al. (2022). Given that extreme events are often influenced by the larger-scale dynamics of the atmosphere, NWP models are commonly employed to analyze and predict them. However, accurately capturing extreme events that significantly impact wind energy remains a challenge.

Improvements in wind and power predictions extend beyond model settings and can be enhanced by incorporating additional physics. One such path to consider is the impact of wind farms on the atmosphere. In NWP models, wind farms are represented by a wind farm parameterization (WFP). Over the years, different WFP have been proposed. A systematic literature review by Fischereit et al. (2022a) compares 10 existing WFPs. Another path for improving predictions is applying data assimilation (DA) techniques. In this study, we focus on both WFP and DA. By employing WFP, the influence of wind farms on the surrounding atmospheric conditions is accounted for, and consequently, an insight into approximated inter-farm dynamics is possible. The WFP that is currently released in WRF is developed by Fitch et al. (2012), and models the wind farm as a momentum sink and a turbulent kinetic energy (TKE) source. A study by Lee and Lundquist (2017) quantifies wind and power prediction improvements that are achieved by incorporating this WFP. Furthermore, Fischereit et al. (2022b) highlight that the WFP of Fitch et al. (2012) is a suitable state-of-the-art choice for modeling the presence of wind farms in WRF, and is selected in the present work. Overall, WFP has been used in a variety of applications, including wind-wave coupling studies (Porchetta et al., 2021), and assessment of modifications in near-surface environment of thunderstorm outflow boundaries (Tomaszewski and Lundquist, 2021).

Along with model setting and including more physics within WRF, improvements in wind and power predictions can also be achieved via DA techniques. Data assimilation is the process of integrating observed data into a numerical model (Skamarock et al., 2019). We will distinguish between two groups of such techniques: variational DA (Barker et al., 2012) and four-dimensional data assimilation (FDDA or nudging, Liu et al. (2008)). Variational DA is concerned with finding the optimal initial state of the atmosphere (in the case of three-dimensional variational data assimilation (3DVar), Barker et al. (2004)), or with finding the optimal model trajectory (in the case of four-dimensional variational data assimilation (4DVar), Huang et al. (2009); Zhang et al. (2013, 2014)). Both variational techniques rely on minimizing the difference between model forecasts and observations by optimizing a cost function. One work that exploits the benefits of variational data assimilation is by Sun et al. (2022), in which wind speed forecasts are improved when assimilating observations from the nacelle of turbines. In contrast, FDDA operates differently from variational data assimilation: FDDA directly influences the state variables over time in order to match observed data (Reen, 2016), and it is the selected method in this work. In FDDA, the approach is to introduce tendency terms in the model equations to adjust the prognostic variables such as temperature, humidity, and wind components, towards observed values. This approach acts as a controller, rather than a cost function optimizer. This

https://doi.org/10.5194/wes-2023-177
Preprint. Discussion started: 7 March 2024

eawe european academy of wind energy
Open Access WIND ENERGY SCIENCE DISCUSSIONS

makes FDDA much more computationally efficient than variational methods, and this is highly relevant in an operational context (Cheng et al., 2017). A drawback of this method is that only prognostic model variables can be assimilated. Besides observational FDDA/nudging, it is also possible to perform grid nudging and spectral nudging in WRF (Skamarock et al., 2019): these are out of the scope of this work. Several studies have explored the leverage of data assimilation techniques in mesoscale models for wind energy applications. For example, Kosovic et al. (2020) use RTFDDA (real-time FDDA) for local data, integrated with artificial intelligence approaches regarding the conversion from wind to power via machine learning. Nudging techniques are also applied in the onshore study of Cheng et al. (2017) that highlights the effectiveness of FDDA in improving wind energy predictions 0-3 hours ahead for normal weather conditions, using only wind speed observations from wind turbine (WT) anemometers. In that study, the RTFDDA forecasting system is used, and as a NWP model, a customized version of WRF is utilized. Furthermore, the study of Mylonas et al. (2018) performs FDDA/nudging of observations from the offshore meteorological mast FINO3 in the North Sea for wind resource assessment and reanalysis.

Despite the vast research available, to our knowledge, there is no study that combines the benefits of a physics-based WFP and FDDA of local observations offshore in improving wind and power predictions in WRF. This is why we focus on utilizing FDDA in WRF offshore by performing observational FDDA/nudging of horizontal wind components, derived from wind speed and wind direction. The latter are collected by LiDAR (Light Detection and Ranging) profilers, and SCADA (Supervisory Control And Data Acquisition) of wind turbine anemometers at hub height. Furthermore, having prominently situated upstream observations makes FDDA especially advantageous as it provides information on incoming wind conditions in advance, which will be highlighted in this work. With this strategy, we aim to enhance the accuracy of wind and power predictions offshore during extreme events that occurred in February 2022 over the Belgian North sea, namely the storms Dudley, Eunice and Franklin. These events had a significant impact on wind power production (reported for example in Belgian Offshore Platform News (2022)), making them important case studies for exploring possibilities for improving wind and power production predictions. Moreover, in order to gain insight into the FDDA setting, we consider different observational nudging parameters by varying nudging strength and radius of influence of the assimilated observations. To evaluate and verify the performance of the simulations, the results are compared to SCADA using classic metrics from the state-of-the-art handbook on wind forecasting by Yang et al. (2021).

The paper is structured as follows. Section 2 describes the methodology and the configuration of the numerical setup of the WRF model. Section 3 portrays results for different scenarios, and the predictions are verified using MAE (mean absolute error) with respect to observations. Section 4 expresses the conclusions of this paper.

2 Methodology and numerical setup

The NWP model employed in this work is the Advanced Research WRF (ARW) Model (Skamarock et al., 2019), v4.5.1, which is a state-of-the-art mesoscale NWP system available in the public domain. It solves the fully compressible non-hydrostatic Euler equations. WRF has a rich set of physics parameterizations, and has an implemented algorithm to assimilate prognostic model variables such as the horizontal components of wind speed via the FDDA (nudging) technique, as described in

https://doi.org/10.5194/wes-2023-177
Preprint. Discussion started: 7 March 2024

eawe european academy of wind energy
Open Access WIND ENERGY SCIENCE DISCUSSIONS

Skamarock et al. (2019) and Reen (2016). With this algorithm, the numerical solution is nudged towards observations by introducing tendency terms in the model equations as

$$\frac{\partial q\mu}{\partial t}(x,y,z,t) = F_q(x,y,z,t) + \mu G_q \frac{\sum_{i=1}^{N} W_q^2(i,x,y,z,t)(q_o(i) - q_m(x_i,y_i,z_i,t))}{\sum_{i=1}^{N} W_q(i,x,y,z,t)},$$

where q is the quantity being nudged (in this work, horizontal wind components derived from wind speed and wind direction), μ is the dry hydrostatic pressure, F_q are the physical tendency terms of q, G_q is the nudging strength, N is the total number of observations, W_q is the weighing function in space and time, q_o is the observed value of the quantity of interest, and $q(x_i, y_i, z_i, t)$ is its model value. The working principle is of a proportional controller: with the approaching of the model value to its observed value, the nudging tendency term decreases.

2.1 The WRF model configuration

Our study is focused on the Belgian-Dutch wind farm cluster. The setup consists of five nested domains, three of which are identical and innermost. The domains have their names and grid cells as follows. D01: 150×150; D02: 190×190; D03, D04, and D05: 220×190 grid cells; centered at latitude $51.42°$ N and longitude $2.74°$ E, with one-way nesting. The three identical innermost domains will be of main interest, with a size of 680 km by 596 km. The horizontal grid spacing is 18 km for the outer domain, 6 km for the intermediate domain, and 2 km for the three innermost domains. The latter follows the guidelines of Fischereit et al. (2022a) to use horizontal grid spacing of at least 3 to 5 times the wind turbine rotor diameter for the domains where the WFP is active (in this case, the innermost ones). We run the simulations using the three identical domains (with 2 km grid spacing) in the following way: D03 is for simulations without WFP, D04 is for active WFP, and D05 – for active WFP and performing FDDA. The domains are shown in Fig. 1, along with key locations of three LiDARs: at the Westhinder (WHi) platform (Glabeke et al., 2023), and at the Lichteiland Goeree platform (LEG) and Europlatform (EPL) (Wind@Sea project, Wind Energy Research Group at TNO Energy Transition, 2023). Details on the physics parameterizations used in the setup can be found in Table 1, and it is based on Hahmann et al. (2020), Dörenkämper et al. (2020), and Larsén and Fischereit (2021). The Lambert conformal projection is selected. The cumulus scheme is used only on the outermost domain. The purpose of our work offshore with FDDA and with the WFP of Fitch et al. (2012) further requires the introduction of sufficient vertical model levels in order to have a representative description of the wind profile across the rotor, which is done by relying on recommendations from Lee and Lundquist (2017). The TKE advection flag has been switched on, following the recommendations of Archer et al. (2020).

In order to account for farm effects, the fully-commissioned offshore wind farms of interest in the North Sea are also included in our simulations via the WFP of Fitch et al. (2012) in WRF. This group of wind farms consists of 1409 wind turbines (out of 5779 in total in Europe and UK (Hoeser et al., 2022)) within 27 different wind farms that are represented in the setup, in proximity to the Belgian-Dutch cluster. The locations of these wind farms are extracted from Hoeser et al. (2022), and the publicly available dataset of Hoeser and Kuenzer (2022). The details of the different wind farms are summarized in Appendix A, Table A1. Besides wind turbine locations, the WFP requires the power and thrust curves for each wind turbine in order

https://doi.org/10.5194/wes-2023-177
Preprint. Discussion started: 7 March 2024

eawe european academy of wind energy
Open Access WIND ENERGY SCIENCE DISCUSSIONS

Parameterization	Scheme (with option in namelist)	Reference
PBL scheme	MYNN 2.5 level TKE (option 5)	Nakanishi and Niino (2006)
Cumulus	Kain-Fritsch (option 1)	Kain (2004)
Microphysics scheme	Thompson et al. (option 8)	Thompson et al. (2008)
Radiation	RRTMG (option 4)	Iacono et al. (2008)
Land surface model	NOAH LSM (option 2)	Ek et al. (2003)

Table 1. Parameterization options in the present WRF model configuration

to simulate its effects on the atmosphere. These were obtained from a mix of both open (https://www.thewindpower.net/; and WindPRO (EMD-International)), and confidential sources.

The vertical levels are stretched which ensures more levels close to the surface, and there are 80 levels in total (Lee and Lundquist, 2017). The lowest level is at 6 m, with sufficient points across the wind turbine rotor for a typical offshore wind turbine in the Belgian-Dutch cluster. The model pressure top is at 1000 Pa. For time integration, third order Runge-Kutta scheme is used, and for advection – second− to sixth−order schemes. For the model integration, adaptive time stepping is used, with target Courant–Friedrichs–Lewy number of 0.6. For initial and boundary conditions, the Global Forecast System (GFS) 3-hourly data from NCEP's Historical Archive is used, with forecast grids on a 0.25 by 0.25 global latitude longitude grid (National Centers for Environmental Prediction, National Weather Service, NOAA, U.S. Department of Commerce, 2015). The simulated time is from 15 February 2022 to 22 February 2022 including a 12-hour spin-up time. This week includes three extreme events which are detailed in Sect. 2.2.

Additionally, our study investigates different configurations for FDDA with respect to data sources (either LiDAR or SCADA), and the sensitivity of results in one day (17 February, with 12-hour spin-up time also included in this day) to the following nudging parameters: horizontal radius of influence R_{xy}, and nudging strength G_q. The assimilation time window is set as default $\tau = 0.667$ hours (Skamarock et al., 2019). Varying the nudging radius and strength can help gain insight into suitable assimilation strategies and practices for extreme event forecasting in wind energy applications.

2.2 Available offshore observations

The observations used for assimilation and performance evaluation of the simulations are collected by a vertical LiDAR at the Westhinder survey platform (51°23'18.74"N, 02°26'16.18"E), as well as by cup anemometers at the wind turbines' nacelles (SCADA data) that belong to one of the wind farms in the Belgian-Dutch cluster. The LiDAR (ZX 300M) is installed at that platform since August 2021 and has been collecting wind speed and wind direction information since (Glabeke et al., 2023). The LiDAR location is illustrated in Fig. 2: located upstream from the farm of interest, the Westhinder LiDAR is situated at approximately 42 km from the Belgian-Dutch cluster. It measures at 11 different heights (34.5, 44.5, 62.5, 79.5, 104.5, 124.5, 149.5, 174.5, 224.5, 274.5 and 324.5 m) at 1 Hz. The location in which these observations are collected is especially favorable, as the measurements are of free-stream wind, given the predominant South-Westerly winds (shown in the year-long

https://doi.org/10.5194/wes-2023-177
Preprint. Discussion started: 7 March 2024

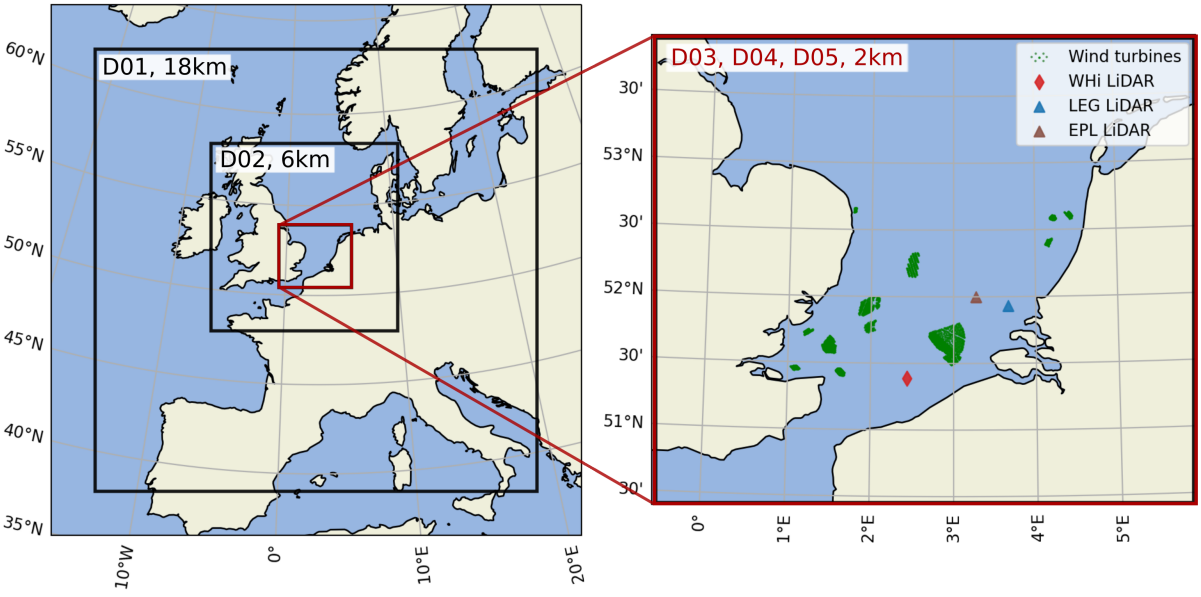

Figure 1. Nested domains in WRF. The domains of interest are the three identical D03, D04, D05, with a grid spacing of 2 km. Key locations that contain observations are indicated (i.e. Westhinder (WHi) LiDAR, LEG and EPL LiDARs). The 1409 wind turbines that are currently included in the WRF setup are also shown on the right.

wind rose in Fig. 2). This allows information to propagate towards the farm of interest when performing FDDA of these local observations. In contrast, the SCADA collects in-situ data at the wind farms on power production, in addition to horizontal wind speed and wind direction. In the present work, we consider 10-minute averages of both SCADA and LiDAR datasets, which both otherwise have a one-second temporal resolution. In order for these observations to be assimilated into WRF, the wind speed and wind direction from the LiDAR and the SCADA at hub heights is pre-processed and translated to horizontal wind components via a standard procedure (Cheng et al., 2017).

To further evaluate our numerical results, we compare also with a LiDAR on the Lichteiland Goeree (LEG) platform (coordinates 51°55′30” N, 3°40′12” E) provided by the Wind@Sea project, Wind Energy Research Group at TNO Energy Transition (2023). The LEG platform is positioned at approximately 30 km South-West from Hoek van Holland, and it collects meteorological observations. Wind speed observations are available and obtained via a Leosphere Windcube LiDAR V2 which can measure up to approximately 250 m above sea level (8 different heights at 62, 90, 115, 140, 165, 190, 215 and 240 m above sea level). This LiDAR is located approximately 63 km further downstream the Belgian-Dutch cluster (see Fig. 2). Finally, we perform comparisons with one more LiDAR dataset that is collected at the Europlatform (EPL) also by the Wind@Sea project, Wind Energy Research Group at TNO Energy Transition (2023) (https://www.tno.nl/, https://nimbus.windopzee.net/). This platform is also located at about 30 km South-West from Hoek van Holland.

https://doi.org/10.5194/wes-2023-177
Preprint. Discussion started: 7 March 2024

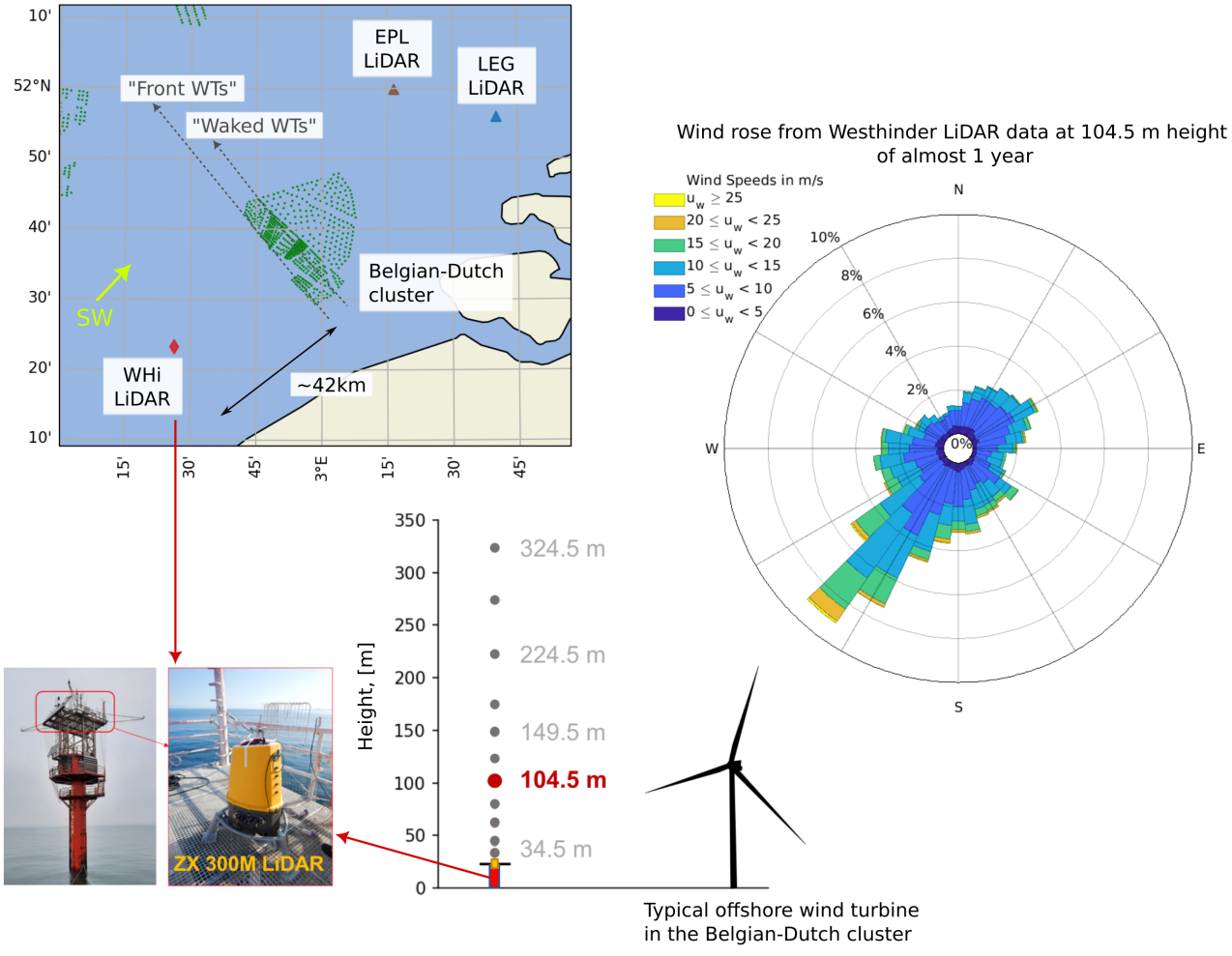

Figure 2. Locations of interest within the innermost domains: the (typically) upstream WHi LiDAR; the "Front WTs" and "Waked WTs" from the Belgian-Dutch cluster (two subsets of 5 wind turbines each); the LEG and EPL LiDARs. An illustration of the LiDAR with respect to a typical wind turbine is shown. On the right: a wind rose obtained from the LiDAR dataset of Glabeke et al. (2023) at 104.5 m above sea level for a period of almost one year (4 August 2021 to 18 July 2022).

2.3 Case studies of extreme events at specific locations

The period of interest in this research is from 15 February 2022 to 22 February 2022. In this period, three extreme events occurred in the Belgian North Sea: the storms Dudley, Eunice, and Franklin. Note that hours in this text and all graphs are always in local time (UTC +1). At the Westhinder (WHi) LiDAR location, according to the observations in Fig. 3, at 104.5 m height, these storms have the following characteristics:

https://doi.org/10.5194/wes-2023-177
Preprint. Discussion started: 7 March 2024

eawe european academy of wind energy
Open Access WIND ENERGY SCIENCE DISCUSSIONS

1. Storm Dudley: afternoon of 16 February – afternoon of 17 February, with a peak velocity of $25.81\ \mathrm{ms}^{-1}$ at 21h on 16 February 2022.

2. Storm Eunice: early morning of 18 February – early morning of 19 February, with a peak velocity of $37.13\ \mathrm{ms}^{-1}$ at 14h on 18 February 2022. Wind direction is overall gradually transient.

3. Storm Franklin: afternoon of 20 February – noon at 21 February, with peak velocity up to $30.46\ \mathrm{ms}^{-1}$ at 19h30 on 20 February 2022. Wind speed and wind direction undergo sharp transitions, especially from 20h00 to 20h30 on 20 February 2022.

We selected this week-long period as it provides versatile atmospheric conditions, including times with values around cut-out wind speed, as well as periods featuring fast changes in wind direction, which can lead to yaw misalignment, making this an interesting case study for FDDA. Data assimilation (FDDA/nudging) is favorable whenever the wind direction is predominantly from South-West, as this allows for the Westhinder LiDAR to be upstream from the Belgian-Dutch cluster. This is most often the case in the Southern Bight of the North Sea, as shown in the wind rose in Fig. 2. Moreover, the LiDAR observations in Fig. 3 evaluate that the average wind direction is from West-Southwest ($247.52°$) for the selected week in February 2022, which is suitable to demonstrate the FDDA capabilities of upstream local data.

The results obtained from the simulations are compared to the five shown locations in Fig. 2: three LiDARs (WHi, LEG, and EPL), as well as two locations with wind turbine data (local wind speed, wind direction, and power) from a SCADA database. The two different locations within the Belgian-Dutch cluster (containing 572 wind turbines) in Fig. 2 are as follows. The first location, “Front WTs”, contains a subset of 5 wind turbines considered as front row with respect to the most common wind direction from South-West (both for the investigated period and overall for the Belgian North Sea, as mentioned previously). The second location, “Waked WTs”, consists of another subset of 5 wind turbines, but they are positioned in the wake (arbitrary back row of a selected Belgian wind farm). In both cases, we consider the average values from the SCADA of the corresponding 5 wind turbines. Having comparisons both in the front and in the wake allows observing the effect of the wind farm parameterization across a few kilometers, as well as the area of impact of the data assimilation upstream.

2.4 Baseline simulations and numerical experiments

The storms are illustrated in a timeline in Fig. 4. We divide the study in two time frames, for which two baseline simulations are always performed: forecasts without WFP and with WFP. Complementing these, depending on the time frame of interest and its goals, we perform numerical experiments of nudging local wind information from either SCADA or LiDAR data source (that is translated into horizontal wind components). The details of all these simulations are listed in Table 2, including their naming, and details on whether WFP is on or off, whether FDDA is performed and if yes, with what properties. In the week-long Frame 1 (F1), we aim to improve predictions via hub-height SCADA FDDA (with a radius of influence $R_{xy} = 4\ \mathrm{km}$) of wind turbine data with respect to SCADA. This is verified at the two selected subsets (front WTs and waked WTs). The expectation is to thus enhance predictions in time for wind speed, wind direction, and power. Furthermore, in a day-ahead Frame 2 (F2), we explore the leverage of having available observations upstream from the Westhinder LiDAR profiler: we assimilate observations at

https://doi.org/10.5194/wes-2023-177
Preprint. Discussion started: 7 March 2024

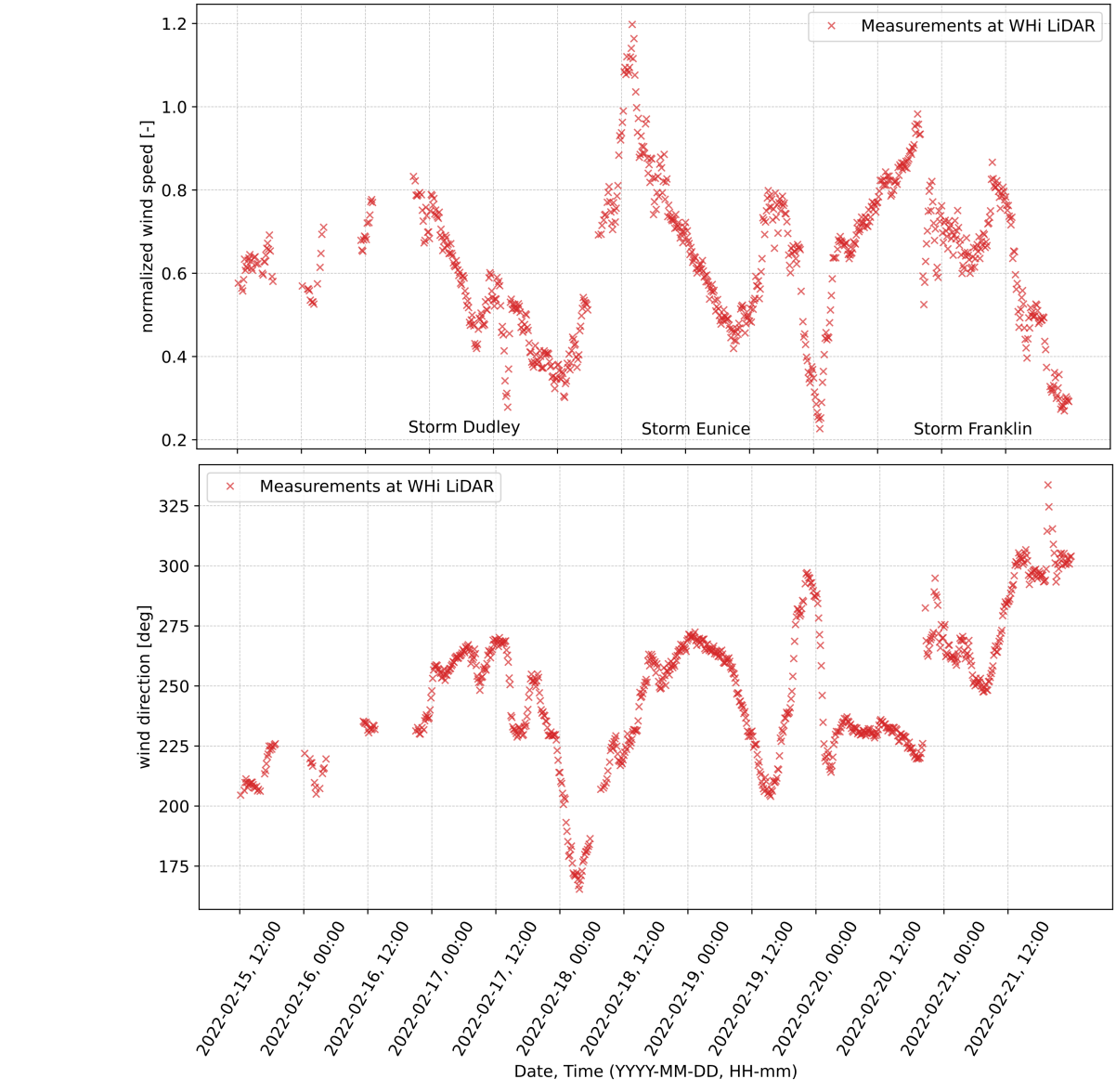

Figure 3. Time series of the LiDAR observations at 104.5 m height during the three extreme events from the Westhinder (WHi) dataset of Glabeke et al. (2023).

200 104.5 m height in all numerical experiments. This is accompanied by a sensitivity study of the results to the radius of influence of observational nudging in FDDA: for the Westhinder LiDAR (being 42 km further), the FDDA experiments are with radius of influence of $R_{xy} = 10$, 20, and 30 km, whereas for the cases of SCADA nudging, values of $R_{xy} = 2$, 4 and 10 km are chosen. Additionally, for the case of FDDA of LiDAR with radius of influence $r = R_{xy} = 20$ km (as in e.g. Cheng et al. (2017)), three values of nudging strength G_q are considered: 6×10^{-4} s^{-1} (a typical value, e.g. in Cheng et al. (2017)), a five times

https://doi.org/10.5194/wes-2023-177
Preprint. Discussion started: 7 March 2024

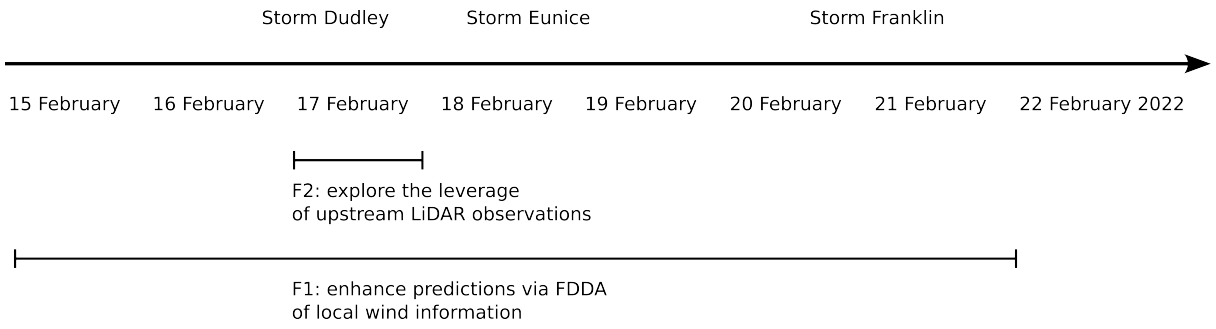

Figure 4. Timeline of the storms. The focus at first is on enhancing predictions via FDDA of SCADA during all three storms (F1, week-ahead). Then – on performing further numerical experiments over one day (F2, day-ahead), aiming to gain insight into favorable FDDA practices.

stronger value of $3 \times 10^{-3}\ \mathrm{s}^{-1}$, and lastly, ten times stronger $G_q = 6 \times 10^{-3}\ \mathrm{s}^{-1}$. After confirming the leverage of the upstream (LiDAR) observations, we propose a simple yet realistic forecasting routine where FDDA of upstream data is performed in a cyclical manner: for a certain amount of time (in this case, one hour window is selected), upstream LiDAR data is assimilated and its effect is propagating as the simulation is running. After this one hour has passed, DA ends and the model continues to run without any further data assimilation, leading to improvements in forecasts solely due to the propagating wind information downstream that is induced by the FDDA effect. For the distance of approximately 42 km from the Westhinder LiDAR to the Belgian-Dutch cluster, this implies 20-70 minutes of advection time and lasting effect of the DA after its end (in this case, one hour). This procedure can be performed as many times as desired (using WRF restart files to ensure the model has spin-up) and improvements can be achieved in any area of interest, as long as the data source is upstream: in this configuration, when the wind is from South-West. All these different numerical experiments yield 3 cases for F1, and 11 cases for F2. All simulations for F1 and F2 with their corresponding names are listed in Table 2.

3 Results and Discussion

This section is dedicated to comparing the results from the simulations at the five locations of interest (the upstream WHi LiDAR; the “Front WTs” and “Waked WTs” at the selected Belgian wind farm; and finally, the two Dutch LiDARs, EPL and LEG). To evaluate simulation performances, we utilize traditional metrics and compare the mean absolute error (MAE, Lydia et al. (2014)) of the different scenarios with respect to the corresponding local observations offshore. MAE is a common evaluation criteria of wind forecasting, as it reflects the overall level of errors (Yang et al., 2021).

3.1 Forecasting with WFP, and enhancing predictions via FDDA of SCADA for week-ahead simulations

Figure 5 illustrates results for F1 (week-ahead) with and without the presence of the wind turbines in the computational domain. It showcases the importance of WFP in WRF by displaying snapshots of wind fields for three arbitrary time slots during this

https://doi.org/10.5194/wes-2023-177
Preprint. Discussion started: 7 March 2024

eawe european academy of wind energy
Open Access WIND ENERGY SCIENCE DISCUSSIONS

Name in graphs	Time period	WFP	FDDA, data source	R_{xy} in km	G_q in s^{-1}
F1: WFP_off	15-22 February	no	no, -	-	-
F1, WFP	15-22 February	yes	no, -	-	-
F1, WFP FDDA, S1	15-22 February	yes	yes, SCADA	4	6×10^{-3}
F2: WFP_off	17 February	no	no, -	-	-
F2, WFP	17 February	yes	no, -	-	-
F2, WFP FDDA, L1	17 February	yes	yes, LiDAR	20	6×10^{-4}
F2, WFP FDDA, L2	17 February	yes	yes, LiDAR	20	3×10^{-3}
F2, WFP FDDA, L3	17 February	yes	yes, LiDAR	20	6×10^{-3}
F2, WFP FDDA, L4	17 February	yes	yes, LiDAR	30	6×10^{-3}
F2, WFP FDDA, L5	17 February	yes	yes, LiDAR	10	6×10^{-3}
F2, WFP FDDA, L6	17 February	yes	yes, cyclic LiDAR	20	6×10^{-3}
F2, WFP FDDA, S1	17 February	yes	yes, SCADA	10	6×10^{-3}
F2, WFP FDDA, S2	17 February	yes	yes, SCADA	4	6×10^{-3}
F2, WFP FDDA, S3	17 February	yes	yes, SCADA	2	6×10^{-3}

Table 2. Details of all simulations performed within F1 (week-ahead 15-22 February 2022), and within F2 (day-ahead 17 February 2022).

period of interest in February 2022. The wind directions for the three snapshots in Fig. 5 are from South-West (top), South (middle), and West (bottom).

For the week-long F1, the time series at the location of the "Waked WTs" are shown in Fig. 6 (both for the cases 'F1, WFP' (a run with active WFP) and 'F1, WFP FDDA S1' (a run with active WFP and with FDDA). For more details on these run, see Table 2). The wind speed values are normalized by cutoff speed. The power is also normalized by the rated values. The forecast using WFP captures well all three storms in F1, as well as swift wind direction changes, especially before Storm Eunice, and before and during Storm Franklin. In order to enhance the modeling during the three extreme events, we perform FDDA of SCADA data every 10 minutes for the whole duration of F1, which provides further improved predictions of wind speed and wind directions, as indicated by the reduced MAE values for the case 'F1, WFP FDDA S1' in Fig. 6.

To evaluate the simulation performances of the different scenarios in the five locations of interest, we present MAEs summarized in Fig. 7, for all three different runs (without WFP, with WFP, and with FDDA of SCADA only) at each location (WHi LiDAR, Front WT, Waked WT, EPL and LEG LiDARs). The predictions at the two wind turbine locations are compared to SCADA data at hub height, whereas the predictions at the three LiDARs are compared to observations at corresponding heights listed in the caption of Fig. 7. Moreover, Fig. 7 emphasizes that WFP helps improve the wind speed, but not the wind direction, whereas further introducing FDDA of SCADA improves both wind speed and wind direction, especially at the wind farm location. At the LiDARs (EPL and LEG, approximately 63 km downstream from the Belgian-Dutch cluster), results remain almost intact. FDDA of in-situ observations such as SCADA provides prediction enhancements which are useful for reanalysis of various events and detailed wind resource assessment, especially if performed for long periods of time.

https://doi.org/10.5194/wes-2023-177
Preprint. Discussion started: 7 March 2024

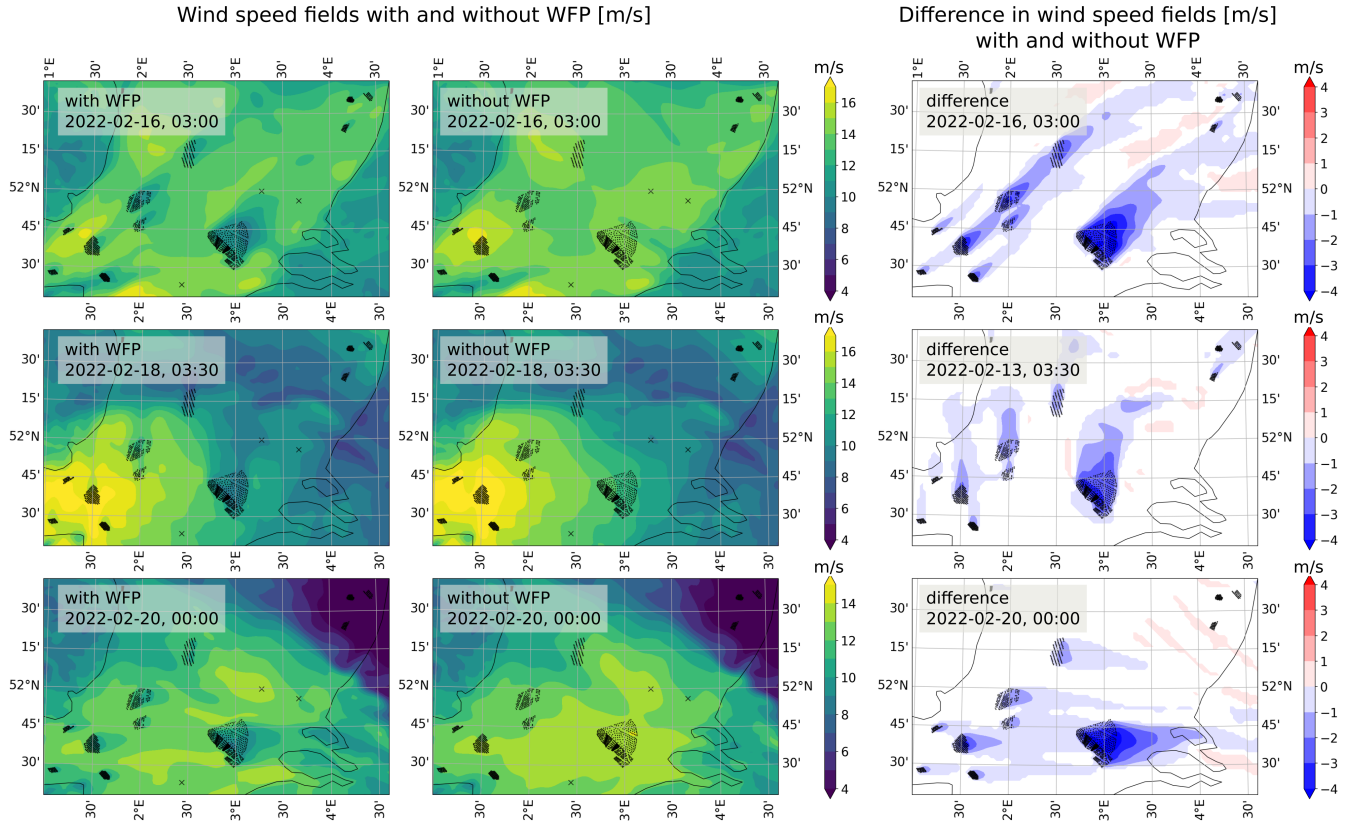

Figure 5. Snapshots of wind speed fields (ms^{-1}) for three different time instances within F1. On the left, results with active WFP show that energy is indeed extracted from the flow. The middle fields are from the simulation without WFP. On the right, the difference in wind speed fields with and without WFP is shown.

3.2 FDDA for day-ahead predictions to leverage available upstream observations

In this section, we perform day-ahead predictions (F2 in Fig. 4) and study the effect of radius of influence of FDDA while nudging either LiDAR or SCADA data. Table 2 can be used as referece as it summarizes all 11 cases of numerical experiments within F2: with and without WFP, nudging LiDAR with different parameters, and nudging SCADA with different radius of influence. For the FDDA of a LiDAR data point at 104.5 m, three values for the radius of influence R_{xy} were tested (10 km, 20 km as in Cheng et al. (2017), and 30 km), whereas for SCADA FDDA – 2 km, 4 km, and 10 km were considered. The configurations offn these 11 cases are detailed in Table 2. FDDA of solely upstream observations (in this case, from the Westhinder LiDAR) has strong advantages, especially being computationally inexpensive and allowing for wind information to propagate to the wind farms in the Belgian-Dutch cluster for (an order of) 20-70 minutes in advance.

Figure 8 shows predictions in the “Waked WTs” location for three variables: wind speed, wind direction, and power. These results are obtained when nudging only LiDAR upstream. The predictions are compared to SCADA data downstream (the

https://doi.org/10.5194/wes-2023-177
Preprint. Discussion started: 7 March 2024

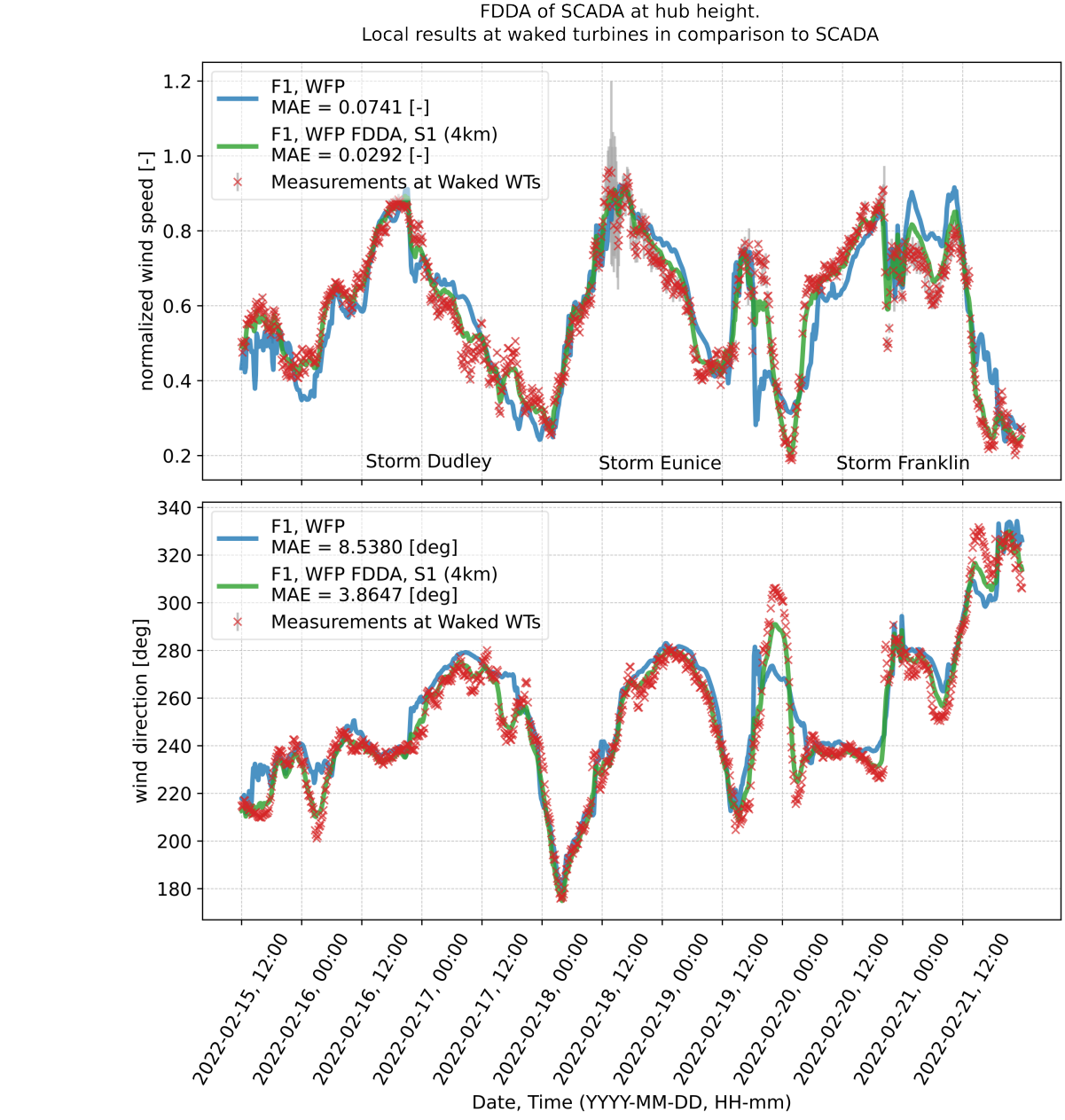

Figure 6. The simulations 'F1, WFP' and 'F1, WFP FDDA S1' when assimilating SCADA at hub height: results at the waked WTs location during the three storms.

average of the observations of the selected subset of turbines in the wake). When performing FDDA of LiDAR, improvements in predictions downstream (at the waked WTs) are evident based on the reduced MAEs in Fig. 8 for wind speed, wind direction and power. Although the LiDAR is located 42 km upstream from the wind farm of interest, the wind direction is favorable

https://doi.org/10.5194/wes-2023-177
Preprint. Discussion started: 7 March 2024

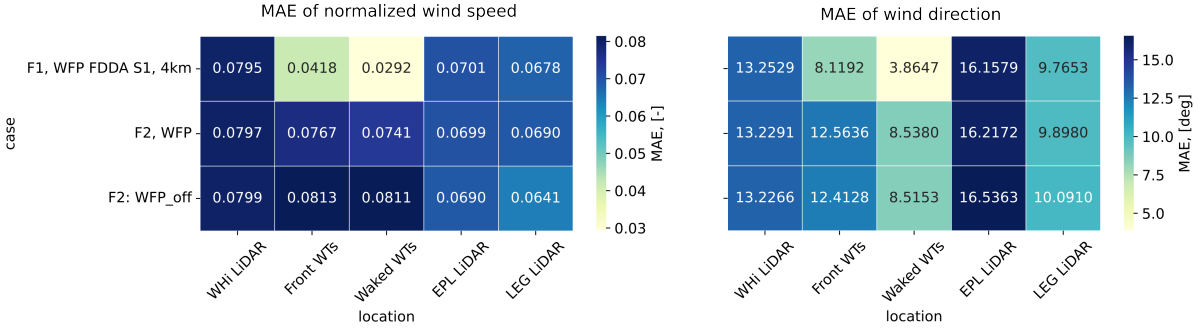

Figure 7. Mean absolute errors (MAEs) computed for each run at five different locations. The errors are estimated with respect to local observations: three LiDAR profilers (WHi at 104.5 m, EPL at 116 m, LEG at 115 m) and two subsets of WTs providing SCADA at hub height.

and from mostly South-West and allows the nudged information to propagate towards the zone of interest (at the Belgian wind farms).

Having upstream observations proves to be especially useful based on the results so far. Therefore, we will now explore a cyclic configuration of FDDA as a forecasting routine. Overall, the use of nudging shows a significant improvement compared to simulations without it. This methodology can be used as long as local observations are available, but in order to utilize this in forecasting mode, it is required to understand the behaviour of the FDDA method when the data stops being fed into the simulation. Therefore, to expose the reach of this method, we will now explore a cyclic numerical experiment of FDDA. We nudge the simulation variables closer to observations in a similar manner as in the previous sections, but only during short periods of time (nudging windows, abbreviated as 'N W'). The assimilation is done again at the WHi LiDAR upstream with a nudging radius of influence of 20 km, as in Cheng et al. (2017). Figure 9 shows the wind speed predictions at the WHi LiDAR (top) while assimilating wind data at a height of 104.5 m in four nudging windows, 1 hour each. The first nudging window (N W1) is from 12:00 h to 13:00 h followed by a forecasting window (FC W1) of 2 hours; the second one (N W2) is from 15:00 h to 16:00 h, and so on. The assimilation window τ during which observations are considered by the model is also indicated in the figure (only in N W3 for illustrative purposes). As expected, we observe that wind speed gets closer to the observations within the nudging time. We also observe in Fig. 9 (bottom) that those quantities still follow better the observations taken downstream even after the end of nudging window. This is explained by the location of the observations with respect to the wind farm. The WHi LiDAR is prominently positioned with respect to the Belgian-Dutch cluster. This allows for the quantities being assimilated during the nudging window to be advected downstream to the wind farm, therefore their values at the wind farm are still influenced after the assimilation has stopped. After the advection time, the simulation resumes back to the reference run with no FDDA. This is especially noticeable 40-50 minutes after the end of a N W due to τ being set at approximately 40 minutes. These lead to improved forecasts downstream at the waked wind turbines, as indicated by the reduced MAE values in in Fig. 9 (bottom). The difference with and without FDDA of upstream LiDAR for the case 'F2, WFP FDDA, L6' can be seen in Fig. 10 for a certain snapshot during this simulation.

https://doi.org/10.5194/wes-2023-177
Preprint. Discussion started: 7 March 2024

eawe european academy of wind energy
Open Access WIND ENERGY SCIENCE DISCUSSIONS

We thus demonstrated a cycling routine with four nudging windows to showcase this effect. With this method for using observations to improve predictions within the hourly range, a LiDAR that is strategically situated (such as in all of these study cases) can become an essential asset for wind farm decision-making, especially for extreme weather events like a storm, or a frontal passage. Due to the enormous impact that this might have for wind farm operators, it can be expected that the use of this method will motivate more measurement campaigns offshore with real-time access. The main limitation of this strategy is when the flow direction is not in its predominant direction, where we would no longer have LiDAR observations upstream; in that case, the wind farm is no longer downstream of the nudged quantity, and therefore remains (almost) unaffected.

To further assess how the F2 day-ahead simulations perform, we compute the MAEs in height with respect to the WHi LiDAR profiles. In Fig. 11, we visualize the MAEs in height for the different simulations (listed in x-axis) that are using LiDAR data (see Table 2). The height of the assimilated LiDAR point is solely at 104.5 m, yet improvements with respect to observations are perceived along the whole profile. A vertical smoothing in wind speed profiles is expressed in this figure which ensures the smooth transition between simulation and observation. Furthermore, the MAEs are reduced for the cases where LiDAR FDDA is performed. The case 'F2, WFP FDDA, L1', that has a typical nudging strength G_q, shows reduction of MAEs of about $1.3 - 1.4$ times for both wind speed and wind direction at 104.5 m. Improvements are especially pronounced when R_{xy} and G_q have higher values. For example, for the case with no data assimilation 'F2, WFP', the MAE of normalized wind speed at the height of 104.5 m is 0.070, whereas when assimilating LiDAR with $R_{xy} = 20$ km in 'F2, WFP FDDA, L3', the MAE is reduced to 0.021 (about 3.3 times). Similarly for these two cases, the MAE of wind direction is reduced about 5.2 times. It is worth remarking also the improvements in the cycling FDDA routine, case 'F2, WFP FDDA, L6', are expressed as MAE reduction for wind speed of about 1.9 times, and for wind direction of about 2.3 times.

Figure 12 compares the MAEs from results at the five locations (with respect to the corresponding local datasets) for the day-ahead predictions for all the cases described in Table 2, namely when not performing any nudging 'F2, WFP_off' and 'F2, WFP', when nudging only LiDAR data 'F2, WFP FDDA, L1-6's, and when nudging only SCADA 'F2, WFP FDDA, S1-3's, all of which have their parameters detailed in Table 2. It is particularly encouraging that performing FDDA of a single LiDAR point (at 104.5 m) upstream from the wind farm zone can lead to improvements in predictions downstream at the wind turbines locations, as seen from the first six rows in Fig. 12, especially in comparison to the last two rows (corresponding to the baseline runs 'F2: WFP_off' and 'F2, WFP'). Performing FDDA of SCADA also enhances (locally) the predictions (the three rows corresponding to 'F2, WFP FDDA, S1-3' with the three different radius of influence 10 km, 4 km, and 2 km. Further downstream at the EPL and LEG LiDARs, the fields are almost unaffected, similarly to the week-long case. Additionally, in Fig. 13, power improvements due to FDDA are also significant and are summarized for all cases that have an active WFP. For normalized power at the Front WTs, the cases of upstream LiDAR data assimilation 'F2, WFP FDDA, L1-6' show a reduced MAE by $1.8 - 2.6$ times in comparison to 'F2, WFP' (without DA), whereas for the cases of SCADA 'F2, WFP FDDA, S1-3' this reduction is of the order of $3.2 - 4.7$ times due to the available in-situ observations.

https://doi.org/10.5194/wes-2023-177
Preprint. Discussion started: 7 March 2024

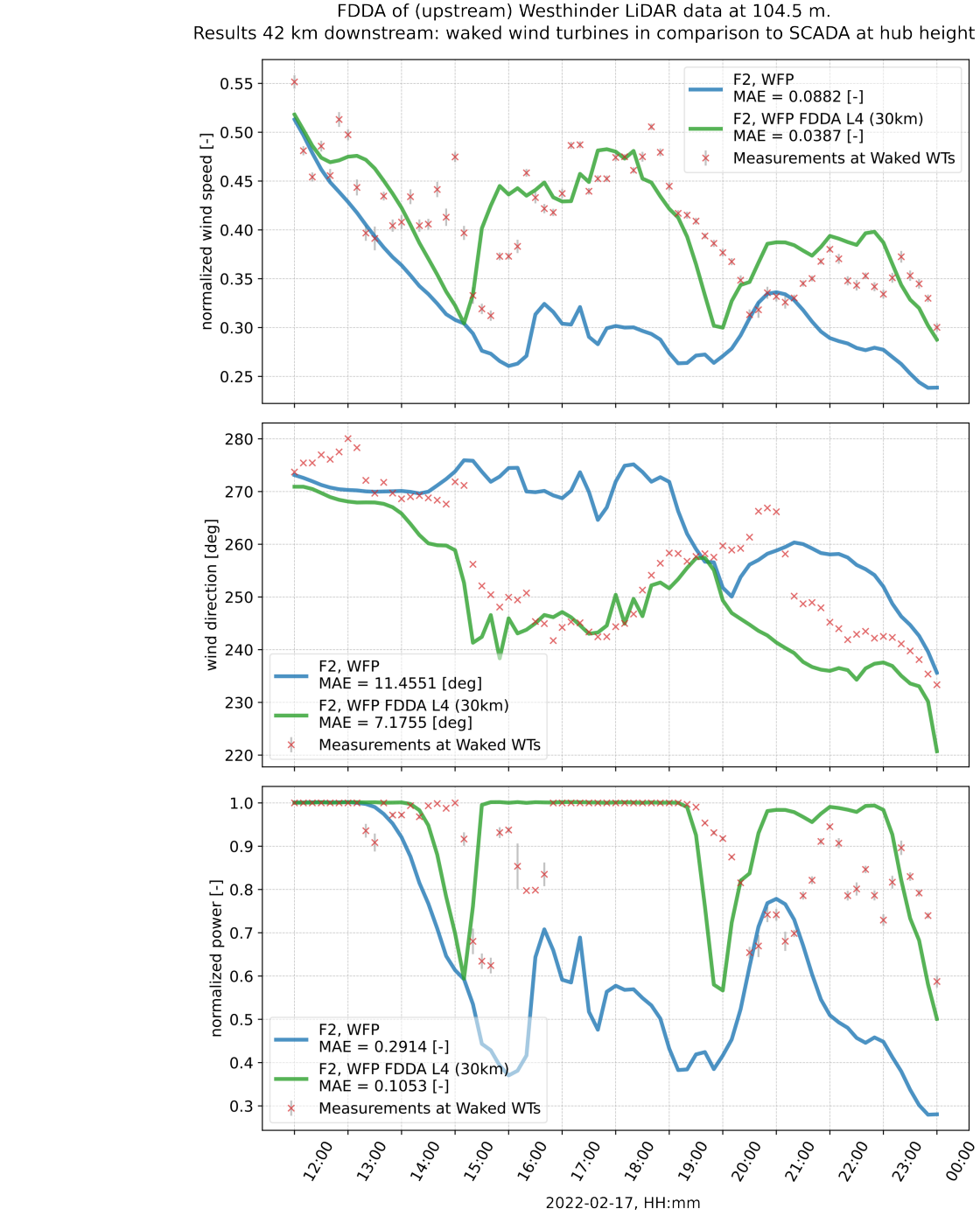

Figure 8. Predictions from the simulations with and without upstream LiDAR FDDA compared to SCADA data downstream from waked WTs. Wind speed (top), wind direction (middle), and power (bottom). Improvements when performing FDDA are highlighted by displaying the MAE values for each variable in the legends.

https://doi.org/10.5194/wes-2023-177
Preprint. Discussion started: 7 March 2024

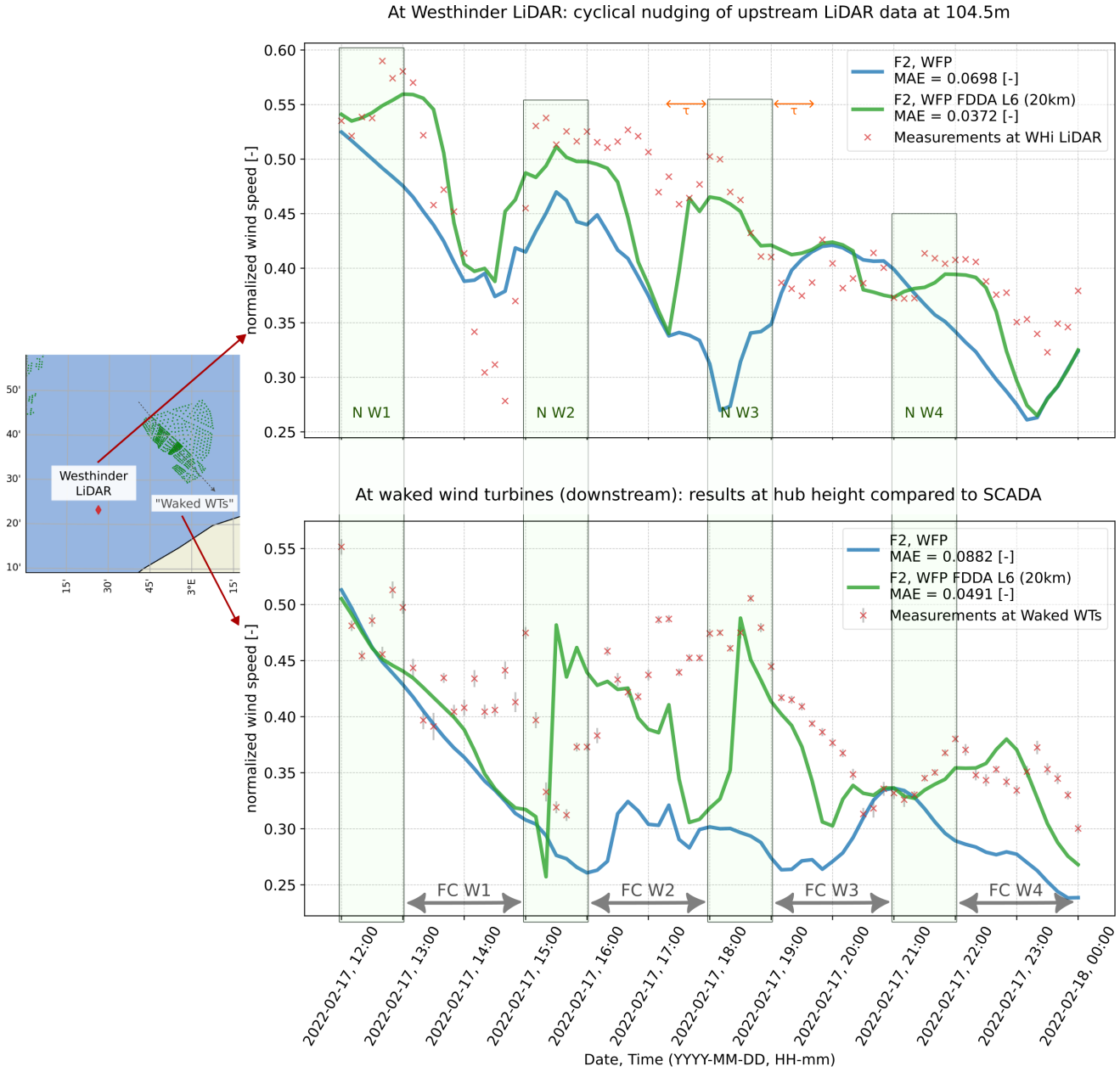

Figure 9. Wind speed predictions at the Westhinder platform, compared to LiDAR data (top), while assimilating wind data at a height of 104.5 m in four nudging windows (N W1-4, one hour each). Information is advected downstream to the location of the waked WTs, and the results are compared to SCADA (bottom). Forecasting windows have a 2-hour length and are denoted as FC W1-4. MAE values are reduced for the case of cyclic nudging in 'F2, WFP FDDA L6' as compared to when no FDDA is performed (in 'F2, WFP').

https://doi.org/10.5194/wes-2023-177
Preprint. Discussion started: 7 March 2024

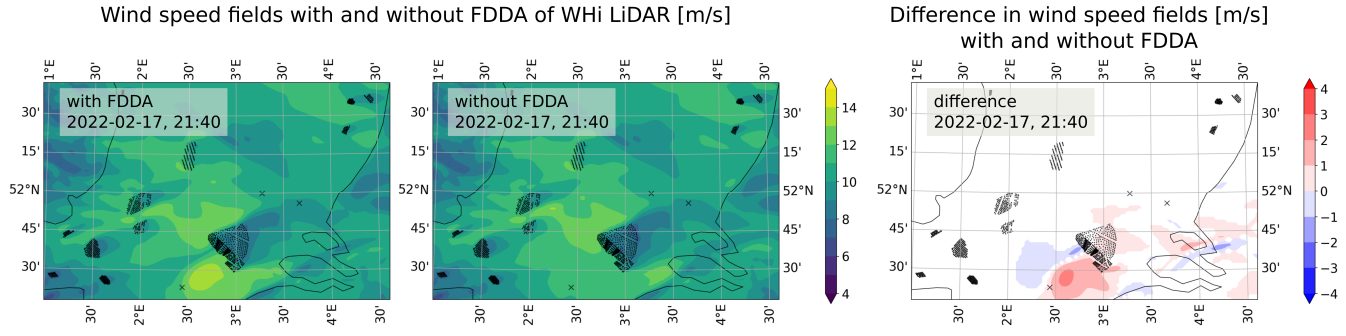

Figure 10. A snapshot of wind speed fields (ms^{-1}) on 17 February 21:40 UTC +1, of 'F2, WFP FDDA, L6' (left) and 'F2, WFP' (without FDDA) (center), as well as the difference between the two (right).

https://doi.org/10.5194/wes-2023-177
Preprint. Discussion started: 7 March 2024

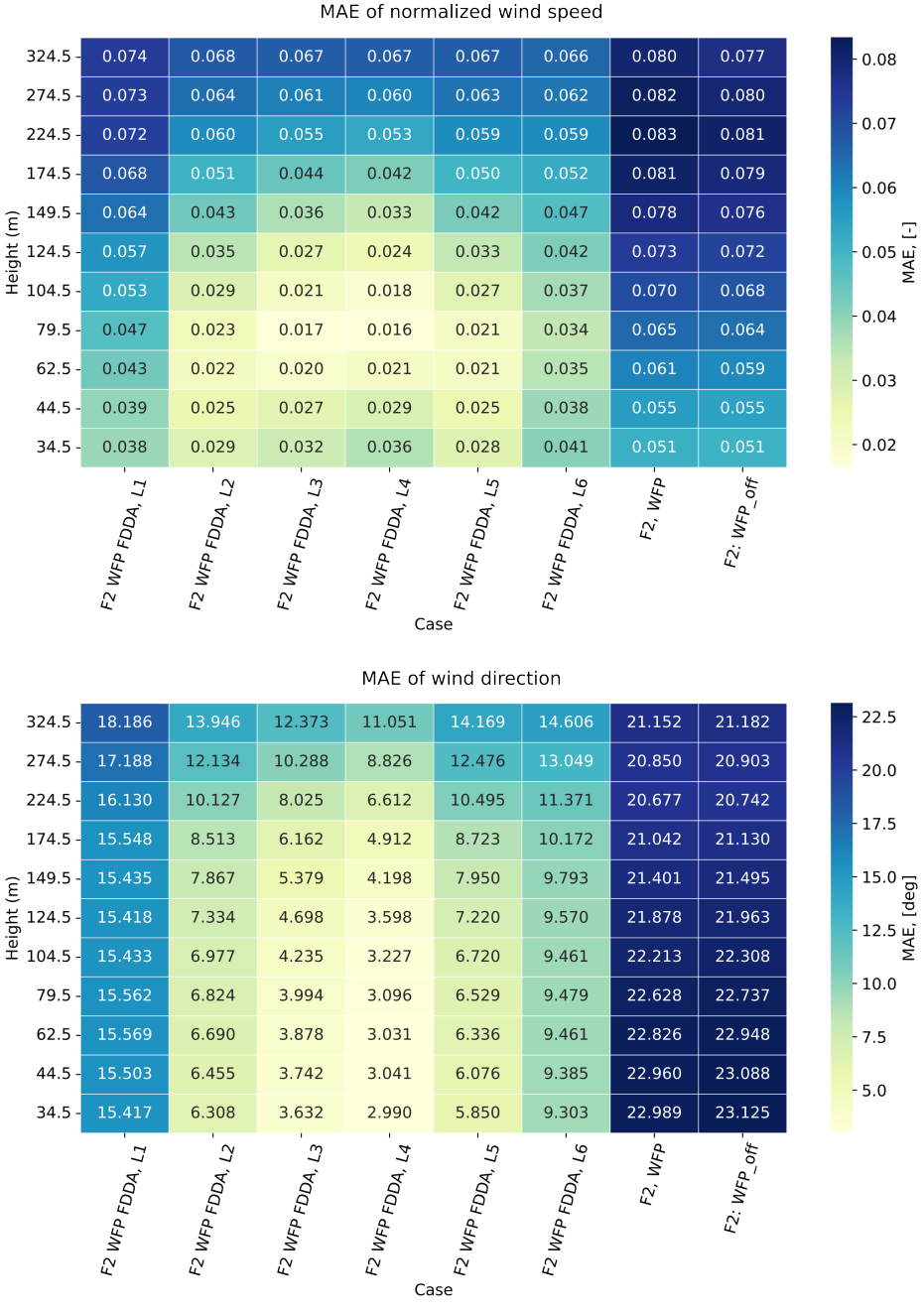

Figure 11. In height: MAEs computed with respect to the LiDAR observations at the Westhinder platform

https://doi.org/10.5194/wes-2023-177
Preprint. Discussion started: 7 March 2024

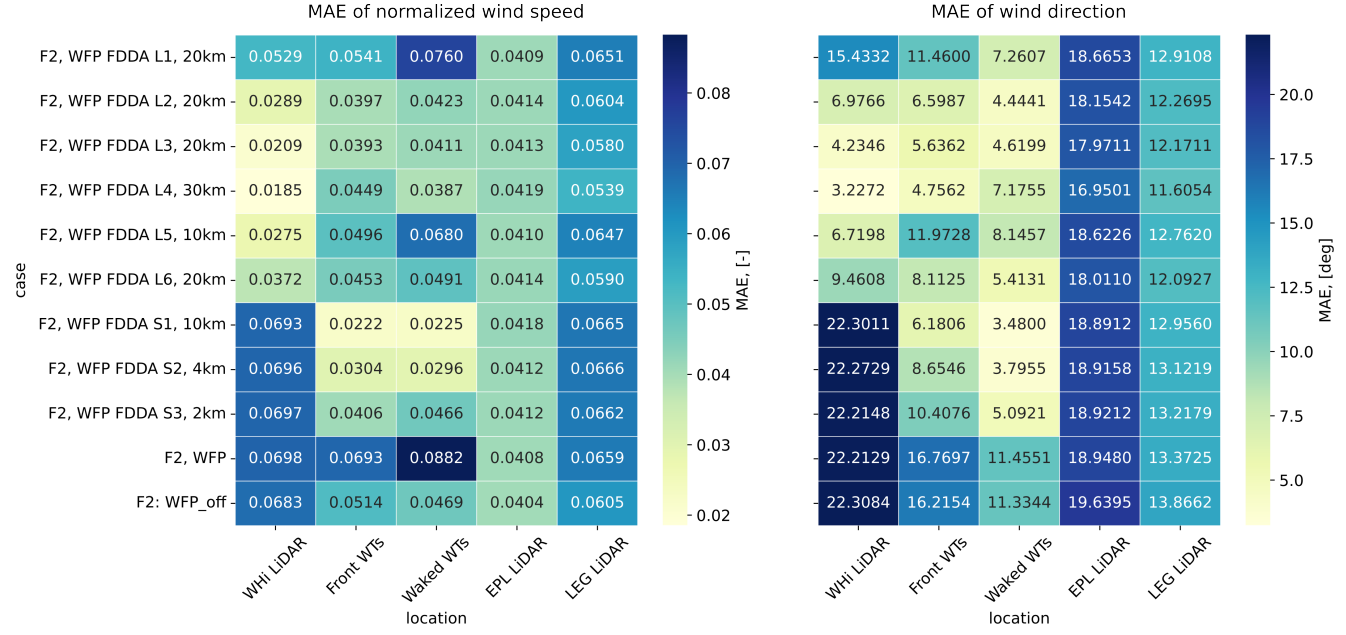

Figure 12. Color maps of MAEs for wind speed and wind direction for the different simulations computed at the five locations with respect to the corresponding observations: WHi at 104.5 m, EPL at 116 m, LEG at 115 m, and Front and Waked WTs at hub height.

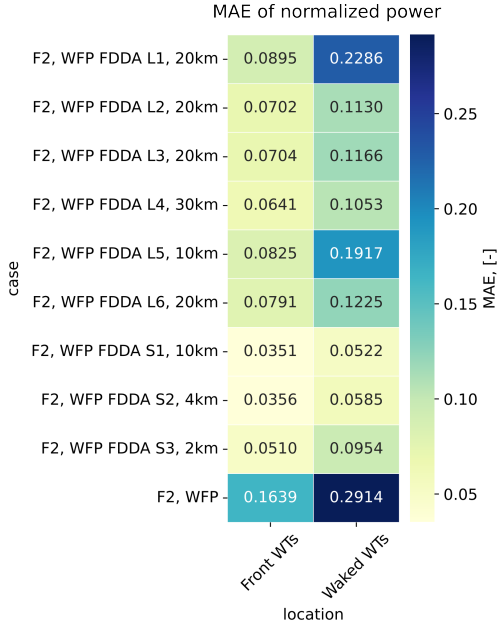

Figure 13. MAEs for normalized power for the different simulations that have an active WFP, computed at the two wind farm locations (front and waked WTs).

https://doi.org/10.5194/wes-2023-177
Preprint. Discussion started: 7 March 2024

4 Conclusions

This study demonstrated the usefulness of assimilating local observations (such as from SCADA or LiDAR) in NWP models (in this case, via FDDA in the Advanced Research WRF model) to improve predictions of wind direction, wind speed and, consequently, power production, based on MAE reduction during a 1-week comparison with three extreme weather events. We forecasted three storms in February 2022 while also representing the wind farms in the domain. The swift nature of these extreme events was captured, and we further enhanced the predictions using FDDA of in-situ (SCADA) observations: improvements were observed regardless of the flow direction.

Moreover, we explored the leverage of the FDDA method in a day-ahead frame by assimilating data either from an upstream (WHi) LiDAR at a specific height, or solely from SCADA at hub height. We performed 11 numerical experiments that have different values for radius of influence of DA, as well as three values for nudging strength. We highlighted the benefits of having an upstream LiDAR, as its assimilation improves predictions downstream at the location of the wind farm. To benefit from this configuration, the only requirement is to have the most common wind direction (for the Southern Bight of the North Sea, this is from South-West) incoming to the Westhinder LiDAR. The experiments of upstream LiDAR DA exhibited improvements in predictions which were quantified by MAEs with respect to the local observations. The MAEs for power production when assimilating upstream LiDAR are reduced approximately twice as compared to the simulations without any DA, whereas this reduction when assimilating SCADA is approximately four times. Furthermore, after demonstrating the leverage of upstream DA, we explored a forecasting routine that contains cyclical nudging windows, which also showed improved forecasts that were quantified via MAEs.

Limitations of this work include the requirement for a specific range of values for wind direction: the assimilation of Westhinder LiDAR data would not show improvements in the downstream region of interest if the wind direction is not from South-West. Additionally, the lack of offshore observations due to the harsh offshore conditions that impact measurement campaigns reduces the geographical areas in which this method can be applied. Another important limitation is that only prognostic variables can be assimilated with the FDDA method, which is why variational methods are widely used and hold potential for future works. Furthermore, the methods in this work can be valuable in the future for operational nowcasting, as well as for long-term reanalysis (several weeks to few years), where the assimilation of offshore data acquired during wind farm pre-development phase can help reduce bias errors and/or reduce the risk of under-sampling extremes, or where the goal is to evaluate the effects of wind farm decommission on present farms.

Practical implications for the wind energy industry can be derived from this research: by utilizing open-source NWP models such as WRF, which is designed for both atmospheric research and operational forecasting applications, more informed planning and decision-making strategies can be pursued, even under extreme weather conditions. This is especially feasible if offshore measurement campaigns continue to be motivated. Furthermore, with the increasing density of wind farms installed in the North Sea, the assimilation of SCADA data from neighboring wind farms in NWP models is an important topic for future research.

https://doi.org/10.5194/wes-2023-177
Preprint. Discussion started: 7 March 2024

eawe european academy of wind energy
Open Access WIND ENERGY SCIENCE DISCUSSIONS

345 *Code and data availability.* The Advanced Research WRF (ARW) model is developed by the National Center for Atmospheric Research, (Skamarock et al., 2019). WRF v4.5.1 is publicly available at https://github.com/wrf-model/WRF/releases/tag/v4.5.1 (last accessed: September 2023). The forcing data used for initial and boundary conditions in the WRF simulations is also publicly available at the NCEP GFS 0.25 Degree Global Forecast Grids Historical Archive, DOI: 10.5065/D65D8PWK. Data from the numerical simulations and the namelists used in the WRF model are available upon reasonable requests. The postprocessing routines are built using the wrf-python library (Lad-
350 wig, 2017). The Westhinder LiDAR data is collected in the framework of the SeaFD project, funded by the Fund for Innovation and Entrepreneurship (VLAIO) at the von Karman Institute for Fluid Dynamics. The LiDAR datasets at the Lichteiland Goeree platform and at the Europlatform are available thanks to the Wind@Sea project, Wind Energy Research Group at TNO Energy Transition (https://www.tno.nl/, https://nimbus.windopzee.net/). Finally, the SCADA observations of the wind farm of interest, as well as details regarding the wind turbines, are under a non-disclosure agreement (NDA).

355 **Appendix A: Included wind farms in the numerical setup**

The included wind farms in the numerical setup are described hereafter, in Table A1, using data from Hoeser et al. (2022) and Hoeser and Kuenzer (2022).

https://doi.org/10.5194/wes-2023-177
Preprint. Discussion started: 7 March 2024

eawe european academy of wind energy
Open Access WIND ENERGY SCIENCE DISCUSSIONS

Wind farm name	**Total number of turbines (#)**	**Turbine Capacity**	**Hub Height** (m)	**Rotor Diameter** (m)
Borssele I Borssele II	94	8.4 MW	107	164
Borssele III Borssele IV	77	9.5 MW	107	164
Borssele V	2	9.5 MW	107	164
Throntonbank I	6	5.0 MW	93.3	126
Throntonbank II & III	48	6.15 MW	93.3	126
Rentel	42	7.35 MW	102	154
Northwind	72	3.0 MW	80.1	112
SeaMade (Seastar)	30	8.4 MW	107	164
Norther	44	8.4 MW	107	164
Nobelwind	50	3.3 MW	77.1	112
Belwind	55	3.0 MW	70.1	112
Belwind Alstom Hailiade	1	6.0 MW	98.1	150
Northwester 2	23	9.5 MW	107	164
Seamade (Mermaid)	28	8.4 MW	107	164
Scroby Sands	30	2.0 MW	68	80
East Anglia ONE	102	7 MW	120	154
Galloper	56	6 MW	88	154
Greater Gabbard	140	3.6 MW	78	107
Gunfleet Sands	48	3.6 MW	78	107
Gunfleet Sands	2	6 MW	84	120
London Array	175	3.6 MW	87	120
Kentfish Flats	30	3 MW	70	90
Kentfish Flats	15	3.3 MW	83.6	112
Thanet	100	3 MW	70	90
Luchterduinen	43	3 MW	81	112
Egmond aan Zee	36	3 MW	70	90
Princess Amalia	60	2 MW	60	80

Table A1. Details on wind farms (lsited in no particular order) in the Southern Bight of the North Sea summarized from Hoeser et al. (2022).

https://doi.org/10.5194/wes-2023-177
Preprint. Discussion started: 7 March 2024

eawe european academy of wind energy
Open Access WIND ENERGY SCIENCE DISCUSSIONS

Author contributions. Tsvetelina Ivanova: Software (lead); Writing – original draft (lead); Writing – review & editing (equal). Data curation (equal); Formal analysis (equal); Investigation (equal);

Sara Porchetta: Supervision (equal); Methodology (equal); Formal analysis (equal); Investigation (equal); Writing – review & editing (equal).

Sophia Buckingham: Methodology (equal); Funding acquisition (equal); Writing – review & editing (equal).

Jeroen van Beeck: Methodology (equal); Funding acquisition (equal); Writing – review & editing (equal).

Wim Munters: Supervision (lead); Conceptualization (lead); Methodology (equal); Funding acquisition (equal); Writing – review & editing (equal). Data curation (equal); Formal analysis (equal); Investigation (equal);

Competing interests. The authors declare that no competing interests are present.

Acknowledgements. The authors acknowledge the RAINBOW and SeaFD projects, funded by Flanders Innovation & Entrepreneurship (VLAIO) of the Flemish Government. Furthermore, the authors acknowledge support by the BeFORECAST project, which is supported by the Energy Transition Fund of the Belgian Federal Government.

The authors extend their gratitude to Pieter Mathys from the von Karman Institute for the review and support during the preparation of the manuscript. The authors acknowledge and thank Gertjan Glabeke from the von Karman Institute for processing the Westhinder LiDAR data.

Furthermore, the authors express acknowledgements and gratitude to the Wind@Sea project, Wind Energy Research Group at TNO Energy Transition (https://www.tno.nl/, https://nimbus.windopzee.net/), for the available observations at the Lichteiland Goeree platform and at the Europlatform.

The results in this paper are obtained using free and open-source software: the authors extend their gratitude to the communities that have built these powerful tools from which everyone can benefit.

Finally, Tsvetelina Ivanova would like to thank Emmanuel Gillyns from the von Karman Institute, for the valuable feedback regarding the structure of the manuscript.

https://doi.org/10.5194/wes-2023-177
Preprint. Discussion started: 7 March 2024

eawe european academy of wind energy
Open Access WIND ENERGY SCIENCE DISCUSSIONS

References

Archer, C. L., Colle, B. A., Delle Monache, L., Dvorak, M. J., Lundquist, J., Bailey, B. H., Beaucage, P., Churchfield, M. J., Fitch, A. C., Kosovic, B., Lee, S., Moriarty, P. J., Simao, H., Stevens, R. J. A. M., Veron, D., and Zack, J.: Meteorology for Coastal/Offshore Wind Energy in the United States: Recommendations and Research Needs for the Next 10 Years, Bulletin of the American Meteorological Society, 95, 515–519, https://doi.org/10.1175/bams-d-13-00108.1, 2014.

Archer, C. L., Wu, S., Ma, Y., and Jiménez, P. A.: Two Corrections for Turbulent Kinetic Energy Generated by Wind Farms in the WRF Model, Monthly Weather Review, 148, 4823–4835, https://doi.org/10.1175/mwr-d-20-0097.1, 2020.

Barker, D., Huang, X.-Y., Liu, Z., Auligné, T., Zhang, X., Rugg, S., Ajjaji, R., Bourgeois, A., Bray, J., Chen, Y., Demirtas, M., Guo, Y.-R., Henderson, T., Huang, W., Lin, H.-C., Michalakes, J., Rizvi, S., and Zhang, X.: The Weather Research and Forecasting Model's Community Variational/Ensemble Data Assimilation System: WRFDA, Bulletin of the American Meteorological Society, 93, 831–843, https://doi.org/10.1175/bams-d-11-00167.1, 2012.

Barker, D. M., Huang, W., Guo, Y.-R., Bourgeois, A. J., and Xiao, Q. N.: A Three-Dimensional Variational Data Assimilation System for MM5: Implementation and Initial Results, Monthly Weather Review, 132, 897–914, https://doi.org/10.1175/1520-0493(2004)132<0897:atvdas>2.0.co;2, 2004.

Belgian Offshore Platform News: Stormy February drives offshore energy production to new record, Available at: https://www.belgianoffshoreplatform.be/en/news/stormy-february-drives-offshore-energy-production-to-new-record/ (Accessed: August 23rd, 2023), 2022.

Cheng, W. Y., Liu, Y., Liu, Y., Zhang, Y., Mahoney, W. P., and Warner, T. T.: The impact of model physics on numerical wind forecasts, Renewable Energy, 55, 347–356, https://doi.org/10.1016/j.renene.2012.12.041, 2013.

Cheng, W. Y., Liu, Y., Bourgeois, A. J., Wu, Y., and Haupt, S. E.: Short-term wind forecast of a data assimilation/weather forecasting system with wind turbine anemometer measurement assimilation, Renewable Energy, 107, 340–351, https://doi.org/10.1016/j.renene.2017.02.014, 2017.

Dörenkämper, M., Olsen, B. T., Witha, B., Hahmann, A. N., Davis, N. N., Barcons, J., Ezber, Y., Garciá-Bustamante, E., González-Rouco, J. F., Navarro, J., Sastre-Marugán, M., Sile, T., Trei, W., Žagar, M., Badger, J., Gottschall, J., Rodrigo, J. S., and Mann, J.: The Making of the New European Wind Atlas - Part 2: Production and evaluation, Geoscientific Model Development, 13, 5079–5102, https://doi.org/10.5194/gmd-13-5079-2020, 2020.

Ek, M. B., Mitchell, K. E., Lin, Y., Rogers, E., Grunmann, P., Koren, V., Gayno, G., and Tarpley, J. D.: Implementation of Noah land surface model advances in the National Centers for Environmental Prediction operational mesoscale Eta model, Journal of Geophysical Research: Atmospheres, 108, https://doi.org/10.1029/2002jd003296, 2003.

Fischereit, J., Brown, R., Larsén, X. G., Badger, J., and Hawkes, G.: Review of Mesoscale Wind-Farm Parametrizations and Their Applications, Boundary-Layer Meteorology, 182, 175–224, https://doi.org/10.1007/s10546-021-00652-y, 2022a.

Fischereit, J., Hansen, K. S., Larsén, X. G., van der Laan, M. P., Réthoré, P.-E., and Leon, J. P. M.: Comparing and validating intra-farm and farm-to-farm wakes across different mesoscale and high-resolution wake models, Wind Energy Science, 7, 1069–1091, https://doi.org/10.5194/wes-7-1069-2022, 2022b.

Fitch, A. C., Olson, J. B., Lundquist, J. K., Dudhia, J., Gupta, A. K., Michalakes, J., and Barstad, I.: Local and mesoscale impacts of wind farms as parameterized in a mesoscale NWP model, Monthly Weather Review, 140, 3017–3038, https://doi.org/10.1175/MWR-D-11-00352.1, 2012.

https://doi.org/10.5194/wes-2023-177
Preprint. Discussion started: 7 March 2024

Glabeke, G., Buckingham, S., De Mulder, T., and van Beeck, J.: Anomalous wind events over the Belgian North Sea at heights relevant to wind energy, https://zenodo.org/record/8034397, Wind Energy Science Conference 2023 Mini-Symposium 1.5 IEA Wind Task 52: Replacing met masts and Accelerating offshore wind deployment, Submission Number 438, 2023.

Hahmann, A. N., Sile, T., Witha, B., Davis, N. N., Dörenkämper, M., Ezber, Y., Garciá-Bustamante, E., González-Rouco, J. F., Navarro, J., Olsen, B. T., and Söderberg, S.: The making of the New European Wind Atlas - Part 1: Model sensitivity, Geoscientific Model Development, 13, 5053–5078, https://doi.org/10.5194/gmd-13-5053-2020, 2020.

Hoeser, T. and Kuenzer, C.: DeepOWT: A global offshore wind turbine data set, https://doi.org/10.5281/ZENODO.5933967, 2022.

Hoeser, T., Feuerstein, S., and Kuenzer, C.: DeepOWT: A global offshore wind turbine data set derived with deep learning from Sentinel-1 data, https://doi.org/10.5194/essd-2022-115, preprint, 2022.

Huang, X.-Y., Xiao, Q., Barker, D. M., Zhang, X., Michalakes, J., Huang, W., Henderson, T., Bray, J., Chen, Y., Ma, Z., Dudhia, J., Guo, Y., Zhang, X., Won, D.-J., Lin, H.-C., and Kuo, Y.-H.: Four-Dimensional Variational Data Assimilation for WRF: Formulation and Preliminary Results, Monthly Weather Review, 137, 299–314, https://doi.org/10.1175/2008mwr2577.1, 2009.

Iacono, M. J., Delamere, J. S., Mlawer, E. J., Shephard, M. W., Clough, S. A., and Collins, W. D.: Radiative forcing by long-lived greenhouse gases: Calculations with the AER radiative transfer models, Journal of Geophysical Research, 113, https://doi.org/10.1029/2008jd009944, 2008.

Kain, J. S.: The Kain–Fritsch Convective Parameterization: An Update, Journal of Applied Meteorology, 43, 170–181, https://doi.org/10.1175/1520-0450(2004)043<0170:tkcpau>2.0.co;2, 2004.

Kosovic, B., Haupt, S. E., Adriaansen, D., Alessandrini, S., Wiener, G., Monache, L. D., Liu, Y., Linden, S., Jensen, T., Cheng, W., Politovich, M., and Prestopnik, P.: A Comprehensive Wind Power Forecasting System Integrating Artificial Intelligence and Numerical Weather Prediction, Energies, 13, 1372, https://doi.org/10.3390/en13061372, 2020.

Ladwig, B.: wrf-python (Version 1.3.4) [Software], https://doi.org/10.5065/D6W094P1, Boulder, Colorado: UCAR/NCAR, 2017.

Larsén, X. G. and Fischereit, J.: A case study of wind farm effects using two wake parameterizations in the Weather Research and Forecasting (WRF) model (V3.7.1) in the presence of low-level jets, Geoscientific Model Development, 14, 3141–3158, https://doi.org/10.5194/gmd-14-3141-2021, 2021.

Larsén, X. G., Du, J., Bolaños, R., Imberger, M., Kelly, M. C., Badger, M., and Larsen, S.: Estimation of offshore extreme wind from wind-wave coupled modeling, Wind Energy, https://doi.org/10.1002/we.2339, 2019.

Lee, J. C. Y. and Lundquist, J. K.: Evaluation of the wind farm parameterization in the Weather Research and Forecasting model (version 3.8.1) with meteorological and turbine power data, Geoscientific Model Development, 10, 4229–4244, https://doi.org/10.5194/gmd-10-4229-2017, 2017.

Liu, Y., Warner, T. T., Bowers, J. F., Carson, L. P., Chen, F., Clough, C. A., Davis, C. A., Egeland, C. H., Halvorson, S. F., Huck, T. W., Lachapelle, L., Malone, R. E., Rife, D. L., Sheu, R.-S., Swerdlin, S. P., and Weingarten, D. S.: The Operational Mesogamma-Scale Analysis and Forecast System of the U.S. Army Test and Evaluation Command. Part I: Overview of the Modeling System, the Forecast Products, and How the Products Are Used, Journal of Applied Meteorology and Climatology, 47, 1077–1092, https://doi.org/10.1175/2007jamc1653.1, 2008.

Lydia, M., Kumar, S. S., Selvakumar, A. I., and Kumar, G. E. P.: A comprehensive review on wind turbine power curve modeling techniques, Renewable and Sustainable Energy Reviews, 30, 452–460, https://doi.org/10.1016/j.rser.2013.10.030, 2014.

Mylonas, M., Barbouchi, S., Herrmann, H., and Nastos, P.: Sensitivity analysis of observational nudging methodology to reduce error in wind resource assessment (WRA) in the North Sea, Renewable Energy, 120, 446–456, https://doi.org/10.1016/j.renene.2017.12.088, 2018.

https://doi.org/10.5194/wes-2023-177
Preprint. Discussion started: 7 March 2024

Nakanishi, M. and Niino, H.: An Improved Mellor–Yamada Level-3 Model: Its Numerical Stability and Application to a Regional Prediction of Advection Fog, Boundary-Layer Meteorology, 119, 397–407, https://doi.org/10.1007/s10546-005-9030-8, 2006.

National Centers for Environmental Prediction, National Weather Service, NOAA, U.S. Department of Commerce: NCEP GFS 0.25 Degree Global Forecast Grids Historical Archive, https://doi.org/10.5065/D65D8PWK, 2015.

Porchetta, S., Muñoz-Esparza, D., Munters, W., van Beeck, J., and van Lipzig, N.: Impact of ocean waves on offshore wind farm power production, Renewable Energy, 180, 1179–1193, https://doi.org/10.1016/j.renene.2021.08.111, 2021.

Pryor, S. C. and Barthelmie, R. J.: A global assessment of extreme wind speeds for wind energy applications, Nature Energy, 6, 268–276, https://doi.org/10.1038/s41560-020-00773-7, 2021.

Reen, B.: A Brief Guide to Observation Nudging in WRF, 2016.

Sethunadh, J., Letson, F. W., Barthelmie, R. J., and Pryor, S. C.: Assessing the impact of global warming on windstorms in the northeastern United States using the pseudo-global-warming method, Natural Hazards, 117, 2807–2834, https://doi.org/10.1007/s11069-023-05968-1, 2023.

Skamarock, W. C., Klemp, J. B., Dudhia, J., Gill, D. O., Liu, Z., Berner, J., Wang, W., Powers, J. G., Duda, M. G., Barker, D. M., and Huang, X.-Y.: A Description of the Advanced Research WRF Model Version 4.3, https://doi.org/10.5065/1DFH-6P97, 2019.

Soman, S. S., Zareipour, H., Malik, O., and Mandal, P.: A review of wind power and wind speed forecasting methods with different time horizons, in: North American Power Symposium 2010, IEEE, https://doi.org/10.1109/naps.2010.5619586, 2010.

Sun, W., Liu, Z., Song, G., Zhao, Y., Guo, S., Shen, F., , and Sun, X.: Improving Wind Speed Forecasts at Wind Turbine Locations over Northern China through Assimilating Nacelle Winds with WRFDA, Weather and Forecasting, 37, 545–562, https://doi.org/10.1175/WAF-D-21-0041.1, 2022.

Thompson, G., Field, P. R., Rasmussen, R. M., and Hall, W. D.: Explicit Forecasts of Winter Precipitation Using an Improved Bulk Microphysics Scheme. Part II: Implementation of a New Snow Parameterization, Monthly Weather Review, 136, 5095–5115, https://doi.org/10.1175/2008mwr2387.1, 2008.

Tomaszewski, J. M. and Lundquist, J. K.: Observations and simulations of a wind farm modifying a thunderstorm outflow boundary, Wind Energy Science, 6, 1–13, https://doi.org/10.5194/wes-6-1-2021, 2021.

Vemuri, A., Buckingham, S., Munters, W., Helsen, J., and van Beeck, J.: Sensitivity analysis of mesoscale simulations to physics parameterizations over the Belgian North Sea using Weather Research and Forecasting – Advanced Research WRF (WRF-ARW), Wind Energy Science, 7, 1869–1888, https://doi.org/10.5194/wes-7-1869-2022, 2022.

Wind@Sea project, Wind Energy Research Group at TNO Energy Transition: LiDAR measurements at Lichteiland Goeree (LEG) and at Europlatform (EPL), (https://www.tno.nl/, https://nimbus.windopzee.net/), 2023.

Yang, B., Zhong, L., Wang, J., Shu, H., Zhang, X., Yu, T., and Sun, L.: State-of-the-art one-stop handbook on wind forecasting technologies: An overview of classifications, methodologies, and analysis, Journal of Cleaner Production, 283, 124 628, https://doi.org/10.1016/j.jclepro.2020.124628, 2021.

Zhang, X., Huang, X.-Y., and Pan, N.: Development of the Upgraded Tangent Linear and Adjoint of the Weather Research and Forecasting (WRF) Model, Journal of Atmospheric and Oceanic Technology, 30, 1180–1188, https://doi.org/10.1175/jtech-d-12-00213.1, 2013.

Zhang, X., Huang, X.-Y., Liu, J., Poterjoy, J., Weng, Y., Zhang, F., and Wang, H.: Development of an Efficient Regional Four-Dimensional Variational Data Assimilation System for WRF, Journal of Atmospheric and Oceanic Technology, 31, 2777–2794, https://doi.org/10.1175/jtech-d-13-00076.1, 2014.